Cosmic Ray Spectrum and Composition with the Pierre Auger Observatory

C. Di Giulio(1), For The Pierre Auger Collaboration (2),

(1) *INFN Roma Tor Vergata - Rome, Italy,*
(2) *Pierre Auger Observatory, Av. San Martín Norte 304, 5613 Malargüe, Argentina* (*)

Summary. — The Pierre Auger Observatory investigates the origin and nature of Ultra High Energy Cosmic Rays (UHECRs) using a hybrid detector. An introduction to the hybrid detector and a review of selected results are presented with an emphasis on the measurement of the cosmic ray energy spectrum and mass composition.

1. – The Pierre Auger Observatory

UHECRs are detected indirectly through extensive air showers (EAS) induced by primary cosmic rays to achieve a large effective detector volume to compensate for their

(*) Full author list:http : //www.auger.org/archive/authors_2013_02.html

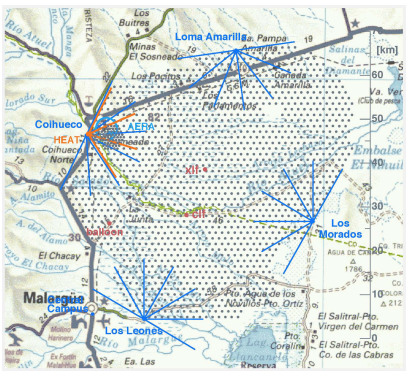

Fig. 1. – The Pierre Auger Observatory located near Malargüe (Mendoza, Argentina). The fluorescence telescope fields of view (blue/orange lines) overlook the water-Cherenkov surface detector array (blue dots).

extremely low flux. UHECR experiments use the atmosphere as a calorimeter and estimate the energy and arrival directions of primary cosmic rays.

Measurements of the energy spectrum, chemical composition (including neutrinos and photons) and arrival directions of UHECRs can provide hints for understanding their origin, propagation and interactions. The Pierre Auger Observatory [1] aims to pursue this goal, with high quality data and unprecedented statistics.

The observatory, located near Malargüe in the province of Mendoza in Argentina (Fig. 1), consists of an array of about 1600 water-Cherenkov Surface Detectors (SD) [2] deployed on the ground over a triangular grid of 1.5 km spacing and covering an area of 3000 km^2. Each SD station is a polyethylene tank of cylindrical shape with size 10 m^2 $\times$ 1.2 m, filled with purified water. Cherenkov light produced by charged particles of EAS in the water is detected by three 9$''$ photomultipliers. Each station is autonomous with a battery and a solar panel. The signals are digitized locally and the information is transmitted via radio to the central data acquisition system. Synchronization is provided by the standard GPS system. The surface detector measures the front of the shower as it reaches the ground. The stations activated by the event record the particle density and the time of arrival.

The ground array is overlooked by 27 fluorescence telescopes, grouped in four sites, making up the fluorescence detector (FD) [3]. In each fluorescence telescope the light is collected by a segmented spherical mirror of area 3.6 m$\times$ 3.6 m through a UV-transparent filter window and a ring corrector lens. Each camera consists of 440 hexagonal photomultipliers, each with a field of view of 1.5°.

The surface array and the fluorescence detector provide complementary measurements of the extensive air showers. The SD samples the density of secondary shower particles at the ground and the total size of the shower is proportional to the energy of the primary cosmic ray. For each event, the particle density is expressed in units of a vertical-equivalent muon (VEM), the average signal produced by vertically incident muons. Measurement of the arrival time of the particles of the shower front at the SD allows one to determine the cosmic ray arrival direction.

The FD observes the longitudinal development of the EAS in the atmosphere by detecting the fluorescence light emitted by de-exitation of nitrogen molecules excited by the charged particles of the shower in air. The result is a measurement of the energy deposit as a function of the atmospheric depth, as in a calorimeter.

As opposed to the SD array, the FD may only operate during clear, moonless nights and its duty cycle is thus reduced to about 13%. Since the fluorescence emission, as well as the light scattering and attenuation, depends on atmospheric conditions, several systems monitor the weather conditions, the aerosol content and the cloud coverage [4].

Events detected by at least one FD telescope and one SD station are named hybrids. The combination of the timing information from the FD and the SD provides an accurate determination of the geometry of the air showers. In fact, in hybrid mode the arrival direction of the primary particle and the impact point of the shower at the ground are determined with a resolution of about 0.6° and 50 m, respectively. A sub-sample of events recorded and independently reconstructed by both FD and SD detectors can be used to calibrate the energy scale of the SD array. This provides an energy parameter only weakly dependent on the primary type and on the hadronic interaction models. Recent results related to the measurement of the energy spectrum and the study of the mass composition are summarized in the next sections. Detailed discussion of other results such as the study of large scale anisotropy [5], the search for point source correlations [6, 7, 8], the measurement of the proton-air cross sections above 10^{18} eV [9], are not reported

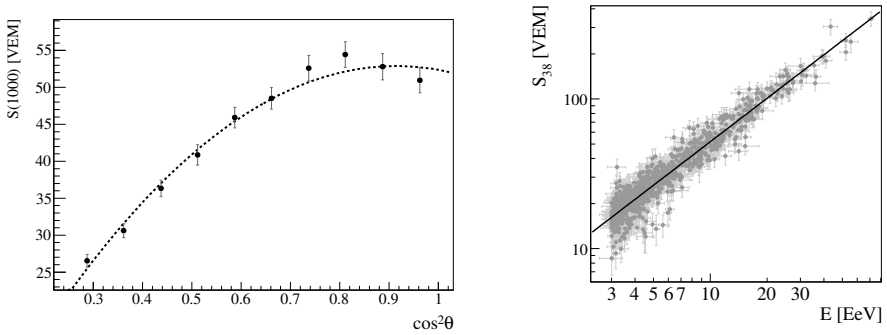

Fig. 2. – On the left, attenuation curve, $CIC(\theta)$, fitted with a second degree polynomial in $x = cos^2\theta - cos^2\theta_{38}$. On the right the correlation between S_{38} and energy (E) for the 839 selected hybrid events used in the fit. The most energetic event shown has an energy of about 75 EeV [10].

here. More details can be found in the corresponding papers.

2. – The SD Energy Calibration

The energy estimator for SD is the signal in VEM, S(1000), at 1000 m from the shower axis, corrected for the shower attenuation in the atmosphere. Assuming an isotropic flux of primary cosmic rays, the shape of the attenuation curve is obtained from the data using the constant intensity cut (CIC) method [10]. To convert S(1000) to $S_{38} = S(1000)/CIC(\theta)$ at the average angle $\theta \simeq 38^\circ$ is taken as a reference, and S_{38} may be regarded as the signal S(1000) the shower would have produced if it had arrived at $\theta = 38^\circ$. To calibrate S_{38} with the energy measured by FD, a subset of 839 high-quality hybrid events (with $E_{FD} > 3$ EeV) has been selected between January 2004 and September 2010.

As shown on the right in Fig. 2, the calibration curve is well described by a single power law function: $E_{FD} = A\, S_{38}^B$ with $A = (1.68 \pm 0.05)\ 10^{17}$ eV and $B = 1.035 \pm 0.009$. This energy calibration has been applied to all SD data collected between January 2004 and December 2010 which were selected with a good geometry and energy reconstruction and had a zenith angle smaller than 60°.

The primary source of systematic uncertainty in the energy spectrum is due to the energy scale [11] (22%). The largest contribution (14%) is given by the absolute fluorescence yield [12]. This contribution will be affected by the recent results of the AirFly Collaboration, which have quoted an uncertainty of 4% on their measurement of the absolute yield [13]. Other contributions are the uncertainties in the absolute calibration of the FD (9%), the measurement of the atmospheric pressure, humidity and temperature (5%), the light attenuation (4-8%, depending on energy), the lateral width and hybrid reconstruction (9%), and the fraction of missing energy (4%).

3. – The measurement of UHECRs Energy Spectrum

The energy spectrum is measured by the Pierre Auger Observatory above an energy threshold of 10^{18} eV and is derived by combining independent measurements in hybrid

and SD modes. The results presented here refer only to the case of events with zenith angles smaller than 60°. More inclined events ($62^\circ < \theta < 80^\circ$) are treated separately because of their different phenomenology. The energy spectrum measured with this category of events [14] is in agreement with the one obtained with other events.

The hybrid spectrum (Fig.3 left) is measured with hybrid events and has been determined using data collected between November 2005 and September 2010. The exposure of the hybrid detector (Fig.4 left) has been determined using time-dependent Monte Carlo simulations taking into account the changing configurations of FD and SD, as well as atmospheric conditions [15, 16].

Only events that satisfy high quality criteria are selected and provide an energy resolution of about 10%. The total systematic uncertainty on the obtained exposure is quoted as 10% at 10^{18} eV and 6% at 10^{19} eV. A total of 3660 good hybrid events have been selected and have been used for the measurement of the energy spectrum above an energy of 10^{18} eV [17].

The exposure for SD spectrum (Fig.4 left) was calculated by integrating the number of active stations of the surface array over time and it is calculated above 3 10^{18} eV where the SD acceptance is saturated independent of the primary mass. It is about 21000 km^2 sr y, as calculated between January 2004 and December 2010, and is known with an uncertainty of about 3%.

The total number of selected events above 3 10^{18} eV (10^{19} eV) is about 64000 (5000) as shown in the SD spectrum (Fig.3 right). The energy resolution is about 16% at threshold, and is about 12% above 10 EeV. A forward-folding approach is thus applied to correct the flux for the energy resolution. This correction is mildly energy dependent but smaller than 20% over the entire energy range. The uncertainty in the normalization of the SD flux is about 6%.

In Fig. 4, on the right, the energy spectrum derived with hybrid data and with the events collected by SD above 3 10^{18} eV are combined together using a maximum likelihood fit. The normalisation uncertainties on the two spectra are used as additional constraints in the combination procedure and a flux scaling factor of 1% has been derived to match the two spectra. Since the SD energy estimator is calibrated from a subset of hybrid events, the two input spectra have the same systematic uncertainty on the energy scale while the flux normalisation uncertainties are independent. The characteristic features of the combined spectrum have been quantified both with three power laws with free breaks between them (dashed line in Fig. 4 right) and with two power laws plus a smoothly changing function (solid line). The parameters are: the energy at which the spectrum has fallen to 1/2 of the value of the power-law extrapolation $E_{1/2}$ and the parametrized width of the transition region W_C. The derived parameters are in Table I with statistical uncertainties. The hypothesis that the power law above the ankle continues to the highest energies with the spectral index γ_2 can be rejected with more than 20 σ. This suppression is compatible with the prediction by Greisen, Zatsepin and Kuz′min (GZK) [18, 19], even if other possibilities cannot be excluded (e.g. limits in the maximum energy at the source).

4. – The measurement of the UHECRs mass composition

The atmospheric depth, X_{max} , at which a shower reaches its maximum development is related to the mass of the primary particle and to the characteristics of the hadronic interactions at very high energy. As FD can directly observe X_{max} , hybrid data (collected between December 2004 and September 2010) are used for this study.

TABLE I. – *Fitted parameters for the spectrum in Fig 4, (right) and their statistical uncertainties characterizing the combined energy spectrum.*

parameter	broken power laws	power laws+ smooth function
$\gamma_1(E < E_{\rm ankle})$	3.27 ± 0.02	3.27 ± 0.01
$\lg(E_{\rm ankle}/{\rm eV})$	18.61 ± 0.01	18.62 ± 0.01
$\gamma_2(E > E_{\rm ankle})$	2.68 ± 0.01	2.63 ± 0.02
$\lg(E_{\rm break}/{\rm eV})$	19.41 ± 0.02	
$\gamma_3(E > E_{\rm break})$	4.2 ± 0.1	
$\lg(E_{\frac{1}{2}}/{\rm eV})$		19.63 ± 0.02
$\lg(W_{\rm c}/{\rm eV})$		0.15 ± 0.02
χ^2/ndof	$37.8/16 = 2.4$	$33.7/16 = 2.1$

The limited field of view of the fluorescence detector and the requirement of observing the shower maximum may introduce a different selection efficiency for different primary masses. To reduce a possible bias, a set of dedicated cuts [20, 21] have been defined to identify the geometrical volume. This guarantees comparable selection efficiency for all nuclear primaries. A total of 6744 events during the declared period (with $E > 10^{18}$ eV) fulfill these criteria and a resolution of about 20 g/cm^2 is derived from simulations and by studying events detected by two FD sites for $X_{\rm max}$.

In Fig.5 the expected $\langle X_{\rm max} \rangle$ for proton and iron primaries, assuming different hadronic interaction models, are shown for reference.

The total systematic uncertainty on $\langle X_{\rm max} \rangle$ is between 10 g/cm^2 at low energy and 13 g/cm^2 at high energy.

The data are well described by a two slope function, with a break point at $log(E/{\rm eV}) = 18.38^{+0.07}_{-0.17}$. The elongation rates derived below and above this energy value are 82^{+48}_{-8} g/cm^2/decade and 27^{+3}_{-8} g/cm^2/decade respectively.

By comparing data and simulations, this result can be interpreted as a change in composition of cosmic rays from light to heavy primaries. However, this conclusion relies

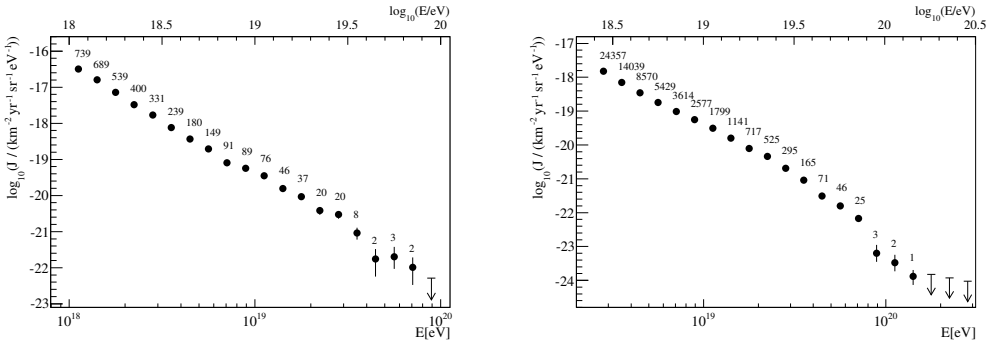

Fig. 3. – On the left: Energy spectrum derived from hybrid data. On the right: Energy spectrum derived from surface detector data calibrated with fluorescence detector measurements. The spectrum has been corrected for the energy resolution of the detector. Only statistical uncertainties are shown and upper limits correspond to 68% CL are shown in both. [17].

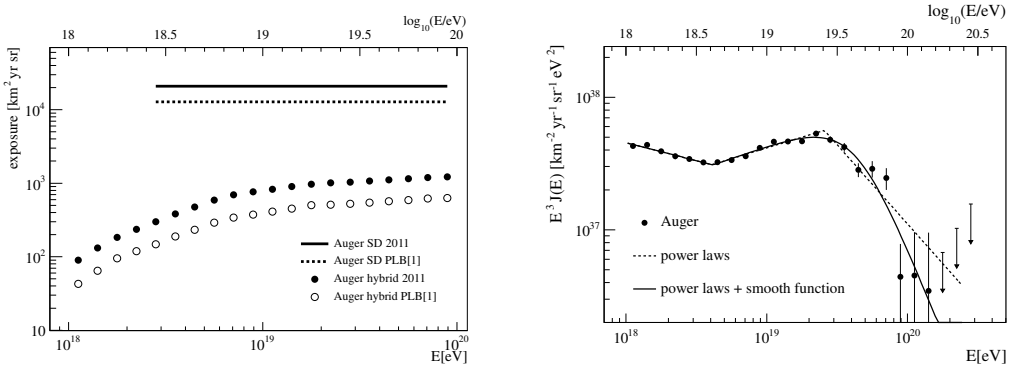

Fig. 4. – On the left the SD and hybrid exposures used for the current flux measurement compared with a previously published data set. The SD exposure is shown for energies higher than $10^{18.5}$ eV where the detector is fully efficient. On the right, the combined energy spectrum is fitted with two functions. Only statistical uncertainties are shown. The systematic uncertainty in the energy scale is 22%.[17].

on the hadronic interaction models, which are based on the extrapolation of accelerator data at lower energies.

The same conclusions can be obtained by investigating the width of the $\langle X_{\rm max}\rangle$ distribution. Fluctuations of the shower development are connected to the mass of the primary type. The RMS($X_{\rm max}$), derived for the same sample of events, is shown in Fig. 5 in the right. The systematic uncertainty has been quoted as 5 g/cm^2. It is clear that the decrease of the RMS($X_{\rm max}$) with energy becomes steeper around the same break point found for the elongation rate.

Moreover, observables from the surface detector that are related to the composition (e.g. muon production depth and azimuthal asymmetry of the signal rise time) provide comparable results [22, 23].

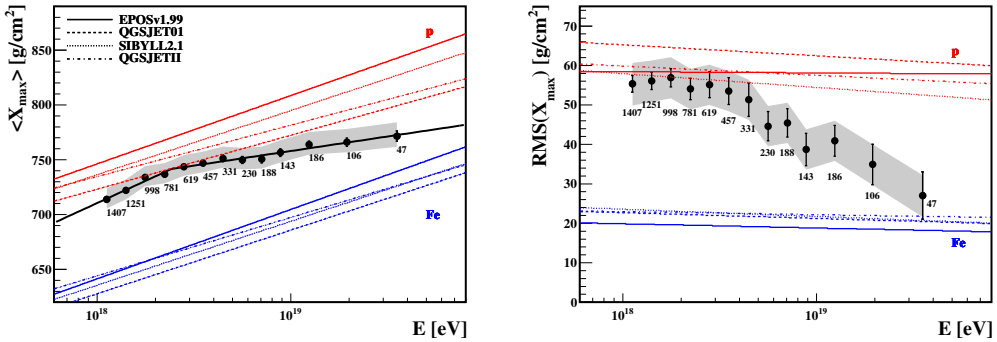

Fig. 5. – On the left $\langle X_{\rm max}\rangle$ is shown as function of the energy. Data (points) are shown together with the predictions for proton and iron for several hadronic interaction models. On the right is shown the RMS($X_{\rm max}$) as a function of the energy. Data (points) are shown with the predictions for proton and iron for several hadronic interaction models. In both figures, the number of events in each bin is indicated and the systematic uncertainties are indicated as a band [21].

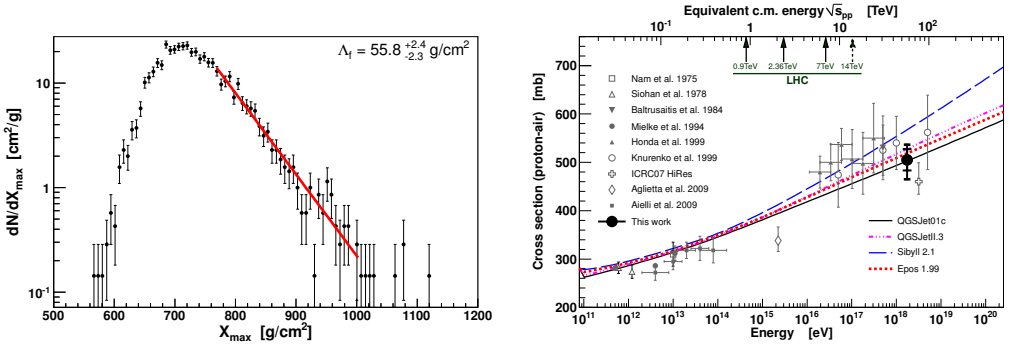

Fig. 6. – On the left, unbinned likelihood fit of Λ_f to the tail of the X_{max} distribution. On the right, the resulting σ_{p-air} is compared to other measurements and model predictions. The inner error bars are statistical only, while the outer include all systematic uncertainties for a helium fraction of 25% and 10 mb photon contamination systematics [9, 30].

As part of the mass composition studies, also non-nuclear components (neutrinos, photons) can be investigated using hybrid events and/or SD events. There is no evidence yet for such non-nuclear components in the Pierre Auger Observatory data (photons [24, 25] and neutrinos [26, 27]).

5. – The proton-air cross-section

Hybrid data provide the possibility to investigate particle interactions at energies well above the limits achievable with the accelerators currently available. The tail of the X_{max} distribution is related to the proton-air cross-section [28, 29]. For this purpose, the shape of the distribution of the largest values of X_{max} is analyzed for a sample of hybrid events. The tail of the X_{max} distribution that contains the 20% of deepest showers exhibits the expected exponential shape $dN/dX_{max} \propto \exp(-X_{max}/\Lambda_f)$, see Fig.6 left. This slope is directly related to the p-air cross-section via $\sigma_{pair} \propto 1/\Lambda_f$. To properly take into account shower fluctuations and detector effects, the exponential tail is compared to Monte Carlo predictions. Any disagreement between data and predictions can then be attributed to a modified value of the proton-air cross-section. In this analysis, the energy interval is restricted to between 10^{18} and $10^{18.5}$ eV, which corresponds to a center-of-mass energy in the nucleon-nucleon system of $\sqrt{s} = 57$ TeV. The interval has been chosen for the high statistics in the data and because the composition is compatible with a dominance of protons. A possible contamination of He primaries could mimic a larger cross-section (e.g. by 20 mb for 20% He contamination) while a photon contamination could reduce the cross-section by at most 10 mb (details in [9, 30]).

At a center of mass energy of 57 ± 6 TeV the $\sigma_{p-air} = 505 \pm 22(stat)^{+28}_{-36}(syst)$ mb The result favors a moderately slow rise of the cross-section towards higher energies, well in line with recent results from LHC ([31, 32, 33]).

6. – Summary

The Pierre Auger Observatory will continue to collect data for several more years to study the nature of the UHECRs with unprecedented precision. A selection of the Pierre Auger Observatory results on the study of the UHECRs have been presented. In

particular the measurement of the energy spectrum with evidence of flux suppression and the study of the mass composition with evidence of a change in composition of cosmic rays from light to heavy primaries and the proton-air cross-section, have been presented.

REFERENCES

[1] Pierre Auger Collab., *Nucl. Instrum. Meth., A*, **523** (2004) 50.
[2] Pierre Auger Collab., *Nucl. Instrum. Meth., A*, **613** (2010) 29.
[3] Pierre Auger Collab., *Nucl. Instrum. Meth., A*, **620** (2010) 227.
[4] Pierre Auger Collab., *Astropart. Phys.*, **33** (2010) 108.
[5] Pierre Auger Collab., *Astrophys. J. Letter*, **762** (2012) L13.
[6] Pierre Auger Collab., *Science*, **318** (2007) 938.
[7] Pierre Auger Collab., *Astropart. Phys.*, **34** (2010) 314.
[8] Pierre Auger Collab., *JCAP*, **04** (2012) 040.
[9] Pierre Auger Collab., *Phys. Rev. Lett.*, **109** (2012) 062002.
[10] R. Pesce, for the Pierre Auger Collab., *Proceedings of the 32nd Int. Cosmic Ray Conf. (ICRC2011) arXiv:1107.4809*, **2** (2011) 145.
[11] C. Di Giulio, for the Pierre Auger Collab., *Proceedings of the 31st Int. Cosmic Ray Conf. (ICRC2009) arXiv:0906.2189*, **2** (2009) .
[12] M. Nagano, K. Kobayakawa, N. Sakaki, and K. Ando,*Astroparticle Physics*, **20** (2003) 293
[13] AirFLY Collab., *Astropart. Phys.*, **42** (2013) 90.
[14] H. P. Dembinski, for the Pierre Auger Collab., *Proceedings of the 32nd Int. Cosmic Ray Conf. (ICRC2011) arXiv:1107.4809*, **2** (2011) 101.
[15] M. Settimo, for the Pierre Auger Collab., *Eur.Phys.J.Plus*, **127** (2012) 87.
[16] Pierre Auger Collab., *Astropart. Phys.*, **34** (2011) 368.
[17] F. Salamida, for the Pierre Auger Collab., *Proceedings of the 32nd Int. Cosmic Ray Conf. (ICRC2011) arXiv:1107.4809*, **2** (2011) 145.
[18] K. Greisen,*Phys. Rev. Lett.*, **16** (1966) 748.
[19] G. T. Zatsepin, V.A. Kuz′min,*Pisma Zh. Eksp. Teor. Fiz.*, **4(3)** (1966) 114.
[20] Pierre Auger Collab., *Phys. Rev. Lett.*, **104** (2010) 091101.
[21] P. Facal, for the Pierre Auger Collab., *Proceedings of the 32nd Int. Cosmic Ray Conf. (ICRC2011) arXiv:1107.4804*, **2** (2011) 105.
[22] D. Garcia-Gamez, for the Pierre Auger Collab., *Proceedings of the 32nd Int. Cosmic Ray Conf. (ICRC2011) arXiv:1107.4804*, **2** (2011) 109.
[23] D. Garcia-Pinto, for the Pierre Auger Collab., *Proceedings of the 32nd Int. Cosmic Ray Conf. (ICRC2011) arXiv:1107.4804*, **2** (2011) 87.
[24] . M. Settimo, for the Pierre Auger Collab., *Proceedings of the 32nd Int. Cosmic Ray Conf. (ICRC2011) arXiv:1107.4805*, **2** (2011) 51.
[25] Pierre Auger Collab., *Astropart. Phys.*, **31** (2009) 399.
[26] Pierre Auger Collab., *Phys. Rev D*, **84** (2011) 102005.
[27] Pierre Auger Collab., *Astrophys. J. Letter*, **L4** (2009) 12001.
[28] R. Ellsworth et al., *Phys. Rev. D*, **26** (1982) 336.
[29] Baltrusaitis et al., *Phys. Rev. Lett.*, **52** (1984) 1380.
[30] R. Ulrich, for the Pierre Auger Collab., *Proceedings of the 32nd Int. Cosmic Ray Conf. (ICRC2011) arXiv:1107.4804*, **2** (2011) 13.
[31] TOTEM Collab., *Europhys. Lett.*, **96** (2011) 21002.
[32] ATLAS Collab., *Nature Commun.*, **2** (2011) 463.
[33] CMS Collab., *arXiv:1205.3142v1*, **05** (2012) .